CONTRAST MEDIA & MOLECULAR IMAGING

Received: 1 March 2013, Revised: 23 May 2013, Accepted: 4 June 2013, Published online in Wiley Online Library

(wileyonlinelibrary.com) DOI: 10.1002/cmmi.1552

New carboxysilane-coated iron oxide nanoparticles for nonspecific cell labelling

Jean-Luc Bridot[a], Dimitri Stanicki[a], Sophie Laurent[a]*, Sébastien Boutry[b], Yves Gossuin[c], Philippe Leclère[d], Roberto Lazzaroni[d], Luce Vander Elst[a] and Robert N. Muller[a,b]

Magnetic resonance imaging (MRI) offers the possibility of tracking cells labelled with a contrast agent and evaluating the progress of cell therapies. This requires efficient cell labelling with contrast agents. A basic incubation of cells with iron oxide nanoparticles (NPs) is a common method. This study reports the synthesis at the gram scale of iron oxide nanoparticles as MRI T_2 contrast agents for cell labelling. These NPs are based on small iron oxide cores coated with a thin polysiloxane shell presenting carboxylic acid functions. The iron oxide cores produced have been characterized by transmission electron microscopy, X-ray diffraction, ζ-potential, infrared, photon correlation spectroscopy, atomic force microscopy, magnetometry and relaxometric measurements. These measurements confirmed the expected surface modification by carboxysilane. Carboxylic groups created electrostatic repulsion between NPs when they are deprotonated. Therefore, highly concentrated aqueous solutions of carboxysilane coated iron oxide NPs can be obtained, up to 70% (w/w). These NPs could be used for cell labelling owing to their aggregation and re-dispersion properties. NPs precipitated in Dulbecco's modified Eagle medium induced a rapid association with 3 T6 fibroblast cells and could easily be re-dispersed in phosphate buffer saline solution to obtain properly labelled cells. Copyright © 2013 John Wiley & Sons, Ltd.

Supporting information may be found in the online version of this article.

Keywords: nanoparticles; iron oxide; cell labelling; ferrofluids; silane; colloidal stability; contrast agent

1. INTRODUCTION

Among their different applications, magnetic nanoparticles used in biomedical research have been developed for detection (1), imaging (2), therapeutic (3) and multimodality purposes (4). Their size is a key factor in their use as probes or as vectors in biological environments because such probes should be at the scale of biological entities in order to facilitate their interaction with cells or biological molecules. These applications are closely dependent on the nanoparticle design and surface modifications. Nanoparticles (NPs) have a great potential for biological applications and, among them, superparamagnetic iron oxide NPs occupy a prominent place owing to their magnetic properties (5). Small iron oxide NPs ($<$20 nm) are superparamagnetic and play an important role in MRI. These nanoparticles induce magnetic field inhomogeneities that speed up the NMR transverse relaxation of water protons, providing a negative contrast in T_2-weighted MRI. As a consequence, the presence of superparamagnetic NPs in an organ causes it to appear darker than surrounding tissue. Because of this property, iron oxide NPs have been widely used in MRI to monitor *in vivo* populations of cells labelled with T_2 contrast agents (6).

In vivo cell tracking by MRI is one of the primary applications of intracellular magnetic labelling (7,8). Basically, intracellular magnetic labelling with iron oxide nanoparticles is achieved by incubating cells in culture with the nanoparticles for a given time. Several strategies, based upon nonspecific uptake mechanisms, are employed to magnetically label cells (6). In this approach, a direct or indirect interaction between the nanoparticles and the cell membrane appears to be a critical step. Both cell type and nanoparticle-related parameters, such as surface properties (nature of the coating and charge, serum protein adsorption) and size (including the formation of aggregates), are determinant parameters for the cellular uptake of magnetic markers (9,10). Prior to be taken off the market for economic reasons, ferumoxides and ferucarbotran [contrast agents for liver MRI approved by the US Food and Drug Administration (FDA)] had become very popular for *in vitro* magnetic cellular labelling applications (11–14). Ferumoxides were often combined with protamine sulfate, an FDA-approved cationic protein used as a heparin antidote (15). Montet-Abou *et al.* demonstrated that the proportion of ferumoxides and protamine

* *Correspondence to: S. Laurent, UMONS, Department of General, Organic and Biomedical Chemistry, NMR and Molecular Imaging Laboratory, B-7000 Mons, Belgium. Email: sophie.laurent@umons.ac.be*

a *J.-L. Bridot, D. Stanicki, S. Laurent, L. Vander Elst, R. N. Muller*
UMONS, Department of General, Organic and Biomedical Chemistry, NMR and Molecular Imaging Laboratory, B-7000 Mons, Belgium

b *S. Boutry, R. N. Muller*
Center for Microscopy and Molecular Imaging, 6041 Charleroi, Belgium

c *Y. Gossuin*
UMONS, Biological Physics Laboratory, B-7000 Mons, Belgium

d *P. Leclère, R. Lazzaroni*
UMONS, Centre for Innovation and Research on Materials and Polymers, Laboratory Chemistry for Novel Materials, B-7000 Mons, Belgium

sulfate must be selected carefully to avoid problems related to complex precipitation (16). Nevertheless, the formation of nanoparticle complexes or agglomerates seems to be a promising pathway for the optimization of cellular magnetic labelling parameters. Indeed it has been observed that cellular uptake is higher when the agglomeration stage of nanoparticles is advanced (17). After interaction of clusters with the cell surface, vesicle formation and subsequent internalization occur (18).

For *in vivo* cell tracking, eliminating the excess of iron oxide material from the cell culture after incubation is crucial to avoid undesired signal voids (i.e. those not owing to exogenously labelled cells). An innovative method should consist of working on a reversible system based on aggregates. First, aggregates made from nanoparticles bearing a charged coating would be formed during the incubation to allow efficient interaction of the magnetic tag with cells and subsequent intracellular uptake. Next, aggregates remaining settled onto the cell layer or plastic/glass bottom of the plate would be dispersed in small clusters or individual NPs and removed during the post-incubation wash. For this reason, it is advantageous to develop NPs presenting low colloidal stability in cell culture media but high stability in phosphate buffered saline (PBS), which is the solution often used to wash cells. To reach this objective, we propose in this work the synthesis of carboxysilane-coated NPs. We first present the process for coating iron oxide NPs by carboxysilane at the gram scale as well as the characterization of coated or uncoated NPs by transmission electron microscopy (TEM), X-ray diffraction (DRX), photon correlation spectroscopy (PCS) and atomic force microscopy (AFM), magnetometry, ζ-potential and relaxometry measurements. Second, we report the cellular labelling strategy in a preliminary observation of cell-associated carboxysilane coated NPs by cytochemical staining of iron on 3 T6 fibroblasts.

2. EXPERIMENTAL SECTION

All chemical compounds were purchased from Aldrich and used as received.

2.1. Synthesis of Iron Oxide NPs

Iron oxide NPs were synthesized using the polyol route (19). An aqueous solution (25 ml) of $FeCl_2 4H_2O$ (0.045 mol) and $FeCl_3$ (0.0375 mol) were added to diethylene glycol (250 ml) under mechanical stirring. The solution was heated to 170 °C and maintained at this temperature for 15 min before adding solid NaOH (0.375 mol). The mixture was maintained at 170 °C under mechanical stirring for 1 h before cooling at 60 °C. Iron oxide NPs were collected with a magnet and washed five times with 100 ml of an HNO_3 solution (1 M). Finally, iron oxide NPs were dispersed with water ($< 25\ \mu S\ cm^{-1}$) in order to constitute the stock solution of NPs.

2.2. Coating of Iron Oxide NPs by Polysiloxane Shell

Iron oxide NPs are coated with a polysiloxane shell composed of TEPSA [3-(triethoxysilyl)propyl succinic anhydride; CAS no. 93642-68-3; Scheme S1 in the Supporting Information] in basic media. NPs were transferred into dimethylformamide (DMF) and water was removed under reduced pressure. 3-(triethoxysilyl)propylsuccinic anhydride (TEPSA, 0.15 mol) was then slowly added to 100 ml of NPs solution in DMF, then 25 ml of water was added, followed by 15 ml of an aqueous solution of tetramethylammonium hydroxide (1 M) at room temperature and under stirring. The solution was heated at 100 °C for 24 h under continuous stirring. NPs were then precipitated by adding an acetone–ether mixture 50:50 (v/v) and collected with a magnet. The precipitate was washed five times with 100 ml of acetone under stirring (10 min) and finally dispersed in water. Afterwards, the solution containing NPs was purified by dialysis against water for 3 days, changing the water bath three times per day.

2.3. Transmission Electron Microscopy

TEM was used to obtain detailed morphological information on the samples and was carried out using a Microscope Fei Tecnai 10 operating at an accelerating voltage of 80 kV (Oregon, USA). The sample was prepared by placing a drop of diluted solution of iron oxide nanoparticle suspension on a grid.

2.4. X-Ray Diffraction

The X-ray diffraction experiments were performed on a D5000 Siemens diffractometer (Karlsruhe, Germany) using the Cu K_α radiation ($\lambda = 0.154056$ nm). The scattering intensities were measured over an angular range of $0 < 2\Theta < 120$ for all samples with a step size (2Θ) of 0.05° and a step time of 25 s.

2.5. Photon Correlation Spectroscopy and ζ-Potential Measurement

The measurements of the size distribution and the ζ-potential of the nanoparticles suspended in aqueous medium were performed on a Zetasizer nano zs (Malvern Instruments) using laser He–Ne (633 nm). The ζ-potential was determined directly in solution containing NaCl (0.01 mM). The pH of the aqueous solution containing NPs was adjusted by adding 0.1–0.001 mM HNO_3 or NaOH solution.

2.6. Fourier Transform Infrared Spectroscopy

Infrared spectra of dried samples were recorded on FTIR spectrometer. The measurements were performed on a Perkin Elmer Spectrum 100 spectrometer (UK) with a solid potassium bromide method, using $2\ cm^{-1}$ resolution and 10 scanning times.

2.7. Atomic Force Microscopy

The surface morphology can be best observed when an AFM apparatus operates in tapping mode (TM), which greatly reduces tip-induced damage. The ultimate resolution of TM-AFM depends on the sharpness of the probe; typically, it is in the order of a few nanometres. AFM was performed on a drop of iron oxide nanoparticle solution deposited on a cleaved mica substrate after solvent evaporation. AFM images were recorded with a Multimode AFM microscope equipped with a Nanoscope V control unit (Veeco, Santa Barbara, CA, USA) running at room temperature in air, using cantilevers with a resonance frequency of about 300 kHz. The working frequency was chosen slightly below the resonance frequency to ensure it was in the repulsive regime and with very low forces during imaging to avoid moving the NPs on the surface. The number of pixels in the images was 512×512.

2.8. Magnetometry

The magnetization curves were recorded on a 50 mM iron solution in a Teflon capsule, with a magnetometer VSM-NUVO (Molspin, Newcastle Upon Tyne, UK) at 25 °C. Magnetizations of the studied materials were obtained after subtraction of the diamagnetic part of the holder sample and the solvent. Magnetizations are expressed as A m^2 kg^{-1} of iron.

2.9. Relaxometry

Proton nuclear magnetic relaxation dispersion profiles extending from 0.23 mT to 1.4 T were recorded at 37 °C on a spinmaster field cycling relaxometer (Stelar, Mede, Italy). Relaxation time measurements (T_1 and T_2) were performed at 37 °C on low-resolution relaxometers operating at 20 and 60 MHz (Minispec mq20 and Minispec mq60, respectively, Bruker, Karlsruhe, Germany).

2.10. Induced Coupled Plasma

Determination of the iron content was performed by Induced coupled plasma–Atomic Emission Spectroscopy (ICP-AES). Samples were dried and solid materials were dissolved in HNO_3 and HCl 1:3 v/v at 60 °C for 1 h before analysis.

2.11. Perl's Cytochemistry of Cell-Associated Iron

3 T6 cells (adherent mouse embryonic fibroblasts) were seeded (2×10^5cells) on sterile glass cover slides to allow microscope observation of cell-associated iron oxide nanoparticles placed in the wells of six-well plates (Greiner, Wemmel, Belgium) and maintained in Dulbecco's modified Eagle medium (DMEM) supplemented with 1% antibiotic–antimycotic solution and 10% heat-inactivated foetal bovine serum (all provided by InvitroGen, Merelbeke, Belgium) in a CO_2 incubator (37 °C, 5% CO_2). The next day, cells were labelled for 4 h with iron oxide nanoparticles coated with carboxysilane (0.5 mM of iron) mixed with 2 ml of serum-free DMEM (to allow nanoparticles agglomeration without influence of serum proteins). After this time, serum-free DMEM was replaced by 2 ml of fresh complete DMEM to restore normal cell growth conditions. After a chase period of 16 h, cells were washed three times with 2 ml of PBS solution. For cytochemical revelation of iron, cells were fixed with 4% formaldehyde prepared in PBS for 15 min and permeabilized with 0.1% triton-100 in PBS for 5 min. Cells were then treated with Perl's reagent (made from equal volumes of 2% potassium ferrocyanide prepared in 2-fold concentrated PBS and 2% HCl in distilled water), and washed with distilled water before counterstaining in aqueous eosin solution. Cover slides are finally mounted in Acrytol (Surgipath, Labonord, Villeneuve D'Ascq, France) on microscope slides. Observations were performed on a Leitz Leica Orthoplan microscope (Wetzlar, Germany) equipped with a Leica DC300F digital camera for recordings.

3. RESULTS AND DISCUSSION

Iron oxide cores were obtained by the polyol method, which consisted of the co-precipitation of metal oxide in high boiling alcohol. The black precipitate of flocculated iron oxide NPs was then washed and suspended in acidic media as previously described in the literature (19).

The TEM picture of the as-prepared particles (Fig. 1) showed spherical objects characterized by a mean size of about 8 nm and by a quite good size homogeneity polydispersity index (PDI 1.38). Characteristic peaks of maghemite were observed by XRD (Fig. S1 in the Supporting Information) and confirmed the inverse spinel structure of these particles.

NPs are characterized by a high surface/volume ratio, up to few hundreds of square metres per gram, which creates a major drawback: NPs tend to agglomerate owing to the short range Van der Waals attractive interaction. Colloidal suspensions are unstable from a thermodynamical point of view but can be stabilized kinetically by the presence of charges and/or polymers inducing electrostatic and/or sterical stabilization (20–23). Uncoated iron oxide nanoparticles present an isoelectric point at neutral pH. To stabilize the iron oxide nanoparticles, TEPSA was used. It is now established that silanol groups react with hydroxyl groups at the iron oxide surface to form a Si–O–Fe link. To have a better control of the hydrolysis of silane's alkoxy groups, the reaction was performed in organic medium in the presence of controlled amount of water. As indicated by TEM (Fig. 1) and XRD (Fig. S1 in the Supporting Information) analysis, the silane treatment of the particles did not lead to a modification of their shape, size nor structure.

The different behaviours of uncoated and coated NPs with respect to the pH are the first indication of the surface modification. Uncoated iron oxide NPs present hydroxyl functions on their surface characterized by a pK_a of 7. At neutral pH, then, the electrostatic repulsion is not sufficient to preserve the colloidal stability of the solution, leading to the precipitation of agglomerated NPs. However, in acidic and basic aqueous media, the protonation and deprotonation of surface hydroxide groups result in colloidal solutions that are electrostatically stabilized by positive or negative charge, as demonstrated by the ζ-potential measurements at different pHs (Fig. 2). Unlike the uncoated NPs, carboxysilaned NPs were stable at neutral pH. The stability domain of coated NPs extends from pH 5 to basic pH. As the pK_a of carboxylic groups is more acidic (pH between 3 and 5) than that of iron oxide surface hydroxide groups (close to 7), carboxysilane coated NPs are stable at neutral pH, as confirmed by the ζ-potential measurements (Fig. 2).

Surface modification was confirmed by FTIR spectroscopy (Fig. S2 in the Supporting Information) by comparing the spectra before and after silane treatment. In the FTIR spectra of TEPSA-modified nanoparticles, we noticed the presence of bands around 2880 cm^{-1} and 1710 cm^{-1}, which can be respectively attributed to C–H and C = O bond vibrations. Bands in the 1000–1200 cm^{-1} region can be attributed to Si–O–Si bond vibrations, confirming the formation of a polysiloxane shell.

Surface modification is also characterized by an increase in the NPs' hydrodynamic diameter (HD). Native iron oxide NPs present a size distribution in intensity characterized by a mean HD of 17.5 nm, while coated ones have an HD of 21.1 nm, as shown in Fig. 3. A difference of 3.6 nm in the HD is thus observed by PCS measurements, which corresponds to an increase in thickness of 1.8 nm, suggesting a thin shell of polysiloxane surrounding the iron oxide core. In number representation, the HDs of uncoated and carboxysilane coated NPs are 9.0 and 12.8 nm respectively.

Except when used in high-resolution mode, transmission electron microscopy (TEM) analysis generally failed to characterize the thin polysiloxane shell owing to the low contrast between polysiloxane and carbon film (Fig. 1). AFM observations were performed on nanoparticles to confirm that they are coated by a thin layer. Uncoated and coated NPs were deposited on a

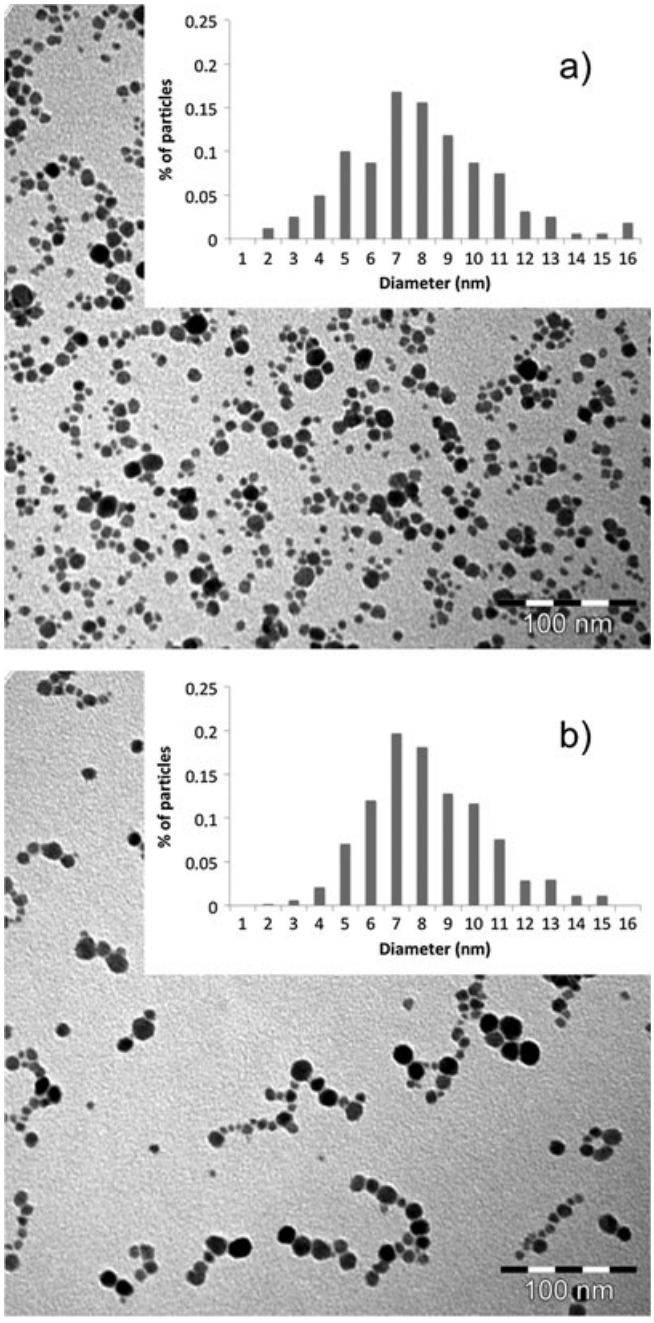

Figure 1. Comparison of transmission electron microscopy pictures of the particles before (a) and after (b) coating by TEPSA.

freshly cleaved mica substrate and the topographies were recorded in tapping mode. The altitude of each spot was measured to determine the size distribution of each kind of NP. The mean size was determined by fitting the experimental data with a log normal function. Size distributions obtained from AFM images (Fig. 4) indicate that iron oxide NPs present one population with a median altitude, h_0, of 9.4 nm ($\sigma = 0.34$) for uncoated and 9.9 nm ($\sigma = 0.23$) for TEPSA-coated NPs. Analyses were performed on all spots present in a $2 \times 2\,\mu m$ field of view, corresponding to 220 and 192 uncoated and coated NPs, respectively. These results confirm that a thin polysiloxane shell is surrounding the iron oxide core. The HD measured by PCS in intensity representation mode was greater than that measured by AFM because this representation mode is very sensitive to large NPs and induces a shift of the mean diameter to larger sizes. The intensity representation mode could be converted into a number representation mode using the Mie theory, which is a more suitable representation mode for techniques such as microscopy (24). In number representation mode, uncoated and coated NPs had HDs of 9.0 nm and 12.8 nm respectively. These values are closer to the AFM distribution results. Even in number representation mode, the hydrodynamic diameter appeared larger than the AFM diameter since the PCS technique measures the hard core surrounded by water molecules and ions of the solvation layer.

Iron oxide NPs developed for biomedical applications such as MRI must remain efficient and preserve their capacity to speed up the relaxation of surrounding protons. In other words, the

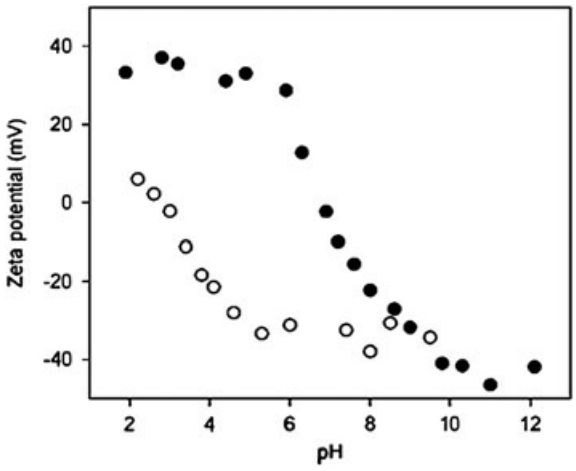

Figure 2. ζ-Potential measurements vs pH of uncoated (solid circles) and carboxysilane coated (open circles) nanoparticles (NPs).

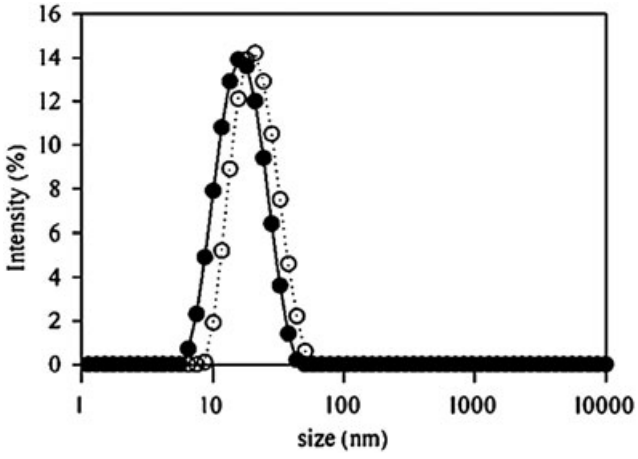

Figure 3. Size distribution in intensity as measured by photon correlation spectroscopy (PCS) of uncoated (solid circles) and carboxy silane coated (open circles) NPs.

coating process must not reduce the relaxation rates of iron oxide NP solutions. Considering an outer sphere mechanism and at high magnetic field, the efficiency of the contrast agent is a function of the radius and the magnetic moment of the nanoparticles which, in turn, is a function of their magnetization (25). Magnetometry of iron oxide NPs renders it possible to determine the saturation magnetization and the size of the superparamagnetic crystals by fitting the data by a Langevin function. The experimental results obtained are characteristic of superparamagnetic NPs. The magnetization curves of uncoated and carboxysilane coated NPs are quite similar (Fig. S3 in the Supporting Information) as well as the parameters provided by the fittings. Iron oxide NPs have a saturation magnetization of around 78.1 A m^2 kg^{-1} of Fe and a diameter of 9.8 nm while iron oxide NPs coated with TEPSA have a saturation magnetization of 84.2 A m^2 kg^{-1} of Fe and a diameter of 10.1 nm. Apparently, the coating process does not significantly modify the magnetic properties, which is appreciable since some coating induces a reduction of the superparamagnetic domain owing to the formation of a spin canting layer near the surface (26). However, if the magnetization of NPs is a significant factor of the transverse relaxivity (r_2) expression, the size of the NPs is another key parameter (27,28). According to the outer sphere theory, the volume surrounding the surperparamagnetic domain must be free so that water molecules can diffuse in order to obtain an optimal efficiency. Increasing the size of nanoparticles without increasing their magnetic moment induces a decrease of the relaxation rate proportional to the r/R ratio where r and R are the radius before and after coating, respectively (29). This assumption is only valid when the particles are in the outersphere relaxation regime.

It appears that the shell must be thin or porous to avoid a reduction of contrast agent efficiency by limiting the access of water protons close to the superparamagnetic cores. A nuclear magnetic resonance dispersion (NMRD) profile was obtained in order to evaluate the relaxometric properties of coated NPs at physiological pH (Fig. 5). NMRD profiles were not obtained for uncoated NPs owing to the lack of stability in solution in the presence of a magnetic field, especially at neutral pH. NMRD profiles show the typical curve expected for superparamagnetic NPs. Fitting was performed using the outer sphere theory with saturation magnetization 58 A m^2 kg^{-1} of Fe, a diameter of the magnetic core of 11.1 nm and a Néel relaxation time of 7.43 10^{-9} s. The size and the saturation magnetization remain compatible with previous data. The size dispersion is responsible for the lower specific magnetization obtained by relaxometry compared with that obtained by magnetometry. Moreover, the small dispersion between 0.1 and 1 MHz and the small r_2/r_1 ratios indicate that carboxysilane coated NPs are well dispersed, confirming thus the absence of aggregates, which is in agreement with the PCS measurements (Fig. 3). Relaxometry at 20 and 60 MHz highlights a high transverse relaxivity value of about 75 s^{-1} mM^{-1} which is similar to commercial compound Sinerem (30).

After synthesis and purification, the batch of carboxysilane-coated NPs can be concentrated by freeze drying and the resulting powder can be easily redispersed by adding water, unlike uncoated NPs, which are not redispersible in water after freeze-drying. By adding small amounts of sodium hydroxide solution and as a result of electrostatic repulsion, it is possible to obtain a highly concentrated ferrofluid, up to 50% in weight of iron oxide, as illustrated by Fig. 6. The iron oxide concentration can be increased up to 70 wt% in water after an additional evaporation step. To reach a high concentration, the percentage of iron oxide in the dried powder must be high. For carboxysilaned NPs, 80 wt% of Fe_2O_3 is obtained in dried powder. Stabilization by steric repulsion has been used by Lee *et al.* to produce iron oxide NPs with a 70 wt% of dried powder (31). As a consequence, to increase the iron oxide content in a solution, a reduction of the size of the NPs or of the coating density is needed. With a short chain of diblock copolymer acrylic acid acrylamide, Jain *et al.* produced aqueous solutions with about 65 and 76 wt% in dried powder (32). While steric repulsion by polymer is the most studied strategy for the stabilization of ferrofluids (33), the present work offers an alternative for the synthesis of highly concentrated ferrofluids, up to 70 wt%, and at the gram scale using electrostatic repulsion by carboxysilane.

Colloidal stability can be evaluated by determining the ζ-potential, which can be defined as the potential value at the shear plane (34). The ζ-potential is expressed as a function of the surface charge density, the diffuse layer thickness depending of the ionic force and the water permittivity. It appears that the

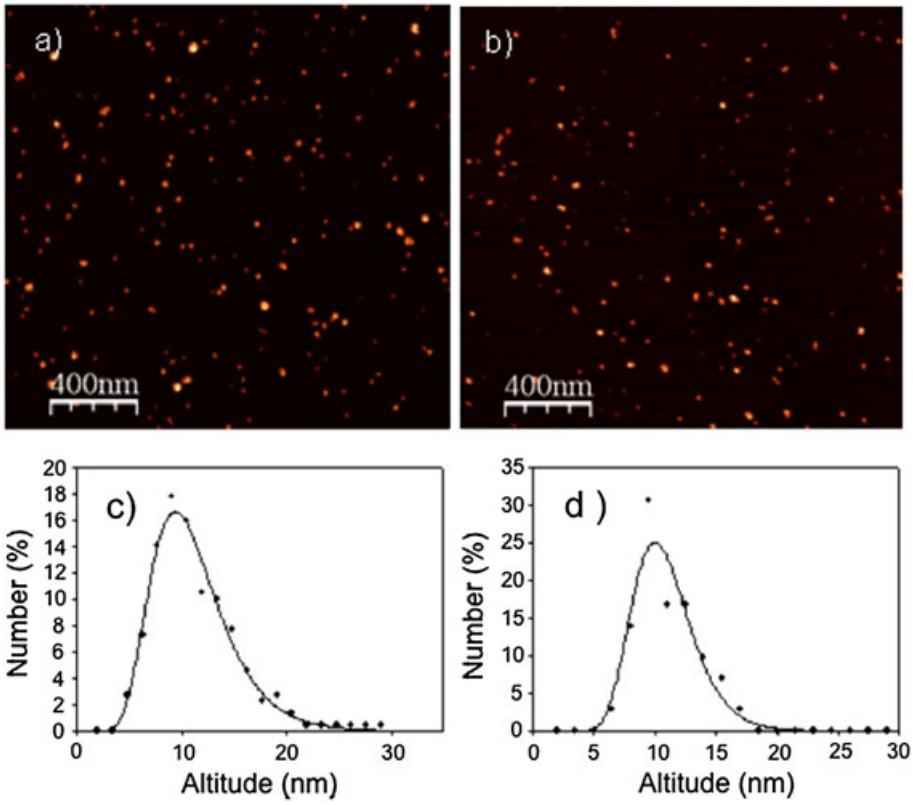

Figure 4. Atomic force microscopy (AFM) images of (a) uncoated and (b) TEPSA-coated NPs and the corresponding altitude distribution of (a) uncoated and (b) TEPSA-coated NPs.

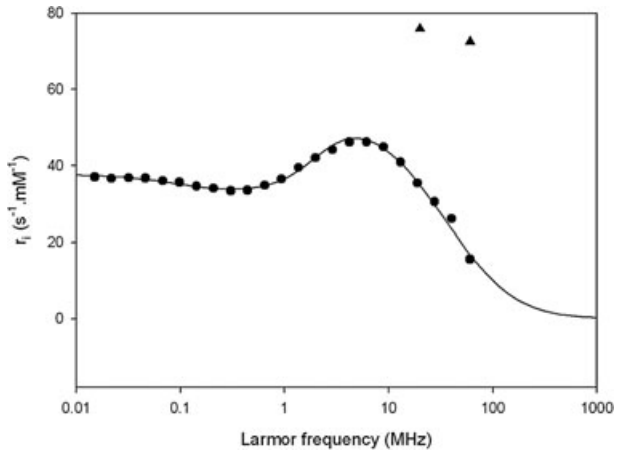

Figure 5. Nuclear magnetic resonance dispersion (NMRD) profile (solid circles) and transverse relaxivities (solid triangles) at 20 and 60 MHz of TEPSA-coated NPs in water.

Figure 6. A 50 wt% aqueous ferrofluid solution of carboxysilane-coated NPs stabilized by electrostatic repulsion with a magnet underneath.

thickness of this layer decreases as the ionic strength increases. This effect is a function of the concentration and the nature of salt in solution. The Gouy Chapman model shows that multivalent ions are more efficient in contracting the layer. Experimentally, the Schulze–Hardy rule shows that the critical coagulation concentration (c.c.c.) depends on the reciprocal charge at power 6. If the colloidal stability depends on many factors, the type of electrolyte and its concentration are crucial. At neutral pH, iron oxide NPs coated with carboxysilane are negatively charged. The charge of NPs is affected by the presence of salts in solution. Adding a salt like NaCl induces a change in ζ-potential value owing to the presence of counter ions on the particle's surface. This effect is generally larger with multivalent ions. Iron oxides coated with carboxysilane are more sensitive to the presence of calcium ions than sodium ions. As a consequence, turbidity appears followed by the precipitation and sedimentation of TEPSA-modified NPs in DMEM medium containing calcium ions. The precipitate formed in DMEM could be redispersed in PBS solution, a medium without calcium ions, after sedimentation and elimination of the supernatant. After a few minutes, the solution is optically clear without any apparent turbidity.

The instability in DMEM and the redispersion of iron oxide nanoparticles coated with TEPSA in PBS was studied by PCS. Figure 7 shows the size distribution results obtained after

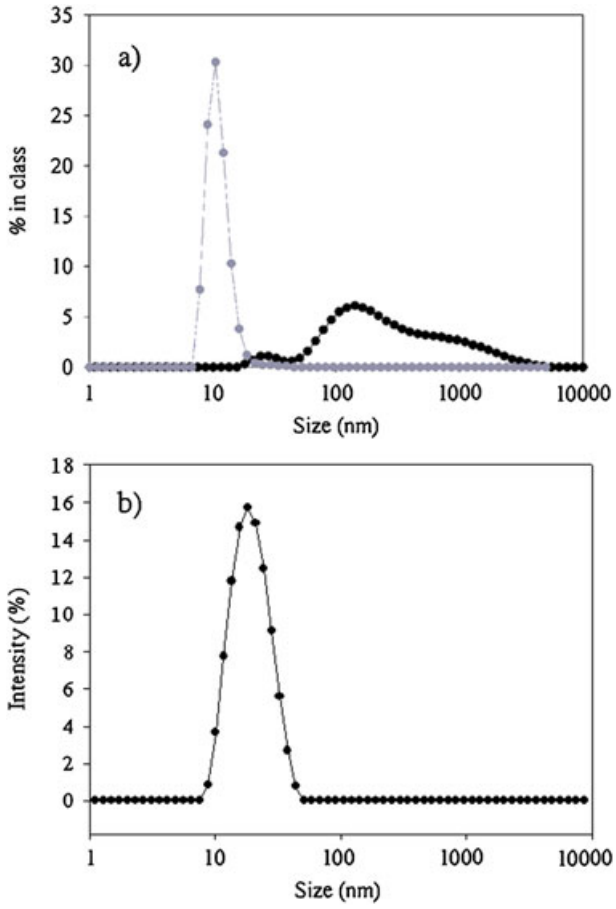

Figure 7. Size distribution for TEPSA NPs obtained by PCS (a) diluted in DMEM after 20 min and expressed in intensity mode (black), in number (grey) and (b) after redispersion in phosphate-buffered saline solution in intensity representation mode.

20 min in DMEM. It illustrates that the number representation mode can mask some aggregation in solution. In this representation mode, there is one peak around 10 nm, in agreement with the size determined in water. However, in intensity mode, large aggregates are observed, up to the micrometric scale. Figure 7 shows the size distribution in intensity representation mode of the solution after precipitation in DMEM for 5 h and redispersion in PBS. A peak at 20 nm is observed and correlates to the size distribution observed before precipitation (Fig. 3), demonstrating the redispersibility of the system.

In comparative studies performed with formerly clinically applicable compounds, ferucarbotran was found to be more efficient than ferumoxides (not complexed with protamine) in labelling cells. It was hypothesized that the negative charges of carboxylate groups in coating were responsible for this efficient uptake (13,14). Cytochemical observations were performed in order to test the feasibility of cellular magnetic labelling based on the formation of carboxysilane-coated nanoparticle aggregates during the incubation, followed by the redispersion of extracellular remaining iron oxide materials during the PBS washing steps. An iron incubation concentration of 0.5 mM allowed nontoxic conditions to be maintained, as suggested by a preliminary tetrazolium assay for cellular viability and activity, in which cells had similar proliferative activity after 24 h incubation with amounts of NPs ranging from 0 to 2 mM Fe (not shown).

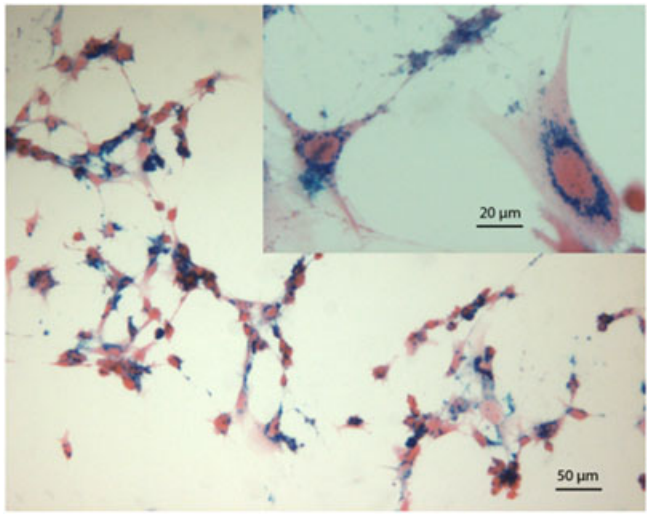

Figure 8. Cytochemical staining of cell-associated iron: 3 T6 fibroblasts (original magnification 10×). Incubation concentration, 0.5 mM Fe in serum-free DMEM. Incubation time, 4 h; chase in complete DMEM, 16 h. In insert, image at higher magnification (original magnification 25×).

Incubation of carboxysilane-coated NPs in DMEM without serum causes the appearance of a turbidity resulting from aggregation. In such a medium, the influence of proteins that could adsorb to nanoparticles is avoided. The sedimentation of aggregates onto cells is expected to facilitate the interaction between iron oxide nanoparticles and the cell membrane, without the need to complex them to a transfection agent as protamine sulfate. Such complexes can indeed be difficult to wash away from the labelled culture, potentially impeding the accuracy of the MRI detection of signal voids upon transplantation of cells in the body. Macrophages could also phagocyte those extracellular complexes and be responsible for undesirable areas of signal darkening (35). Our conditions included a 16 h chase in complete medium to allow the cellular internalization of iron oxide nanoparticles settled onto the membrane in normal cell growth conditions. During washing steps performed afterwards, it was observed that the PBS solution became slightly yellowish, indicating that NPs were dispersed as expected. Figure 8 shows Perl's cytochemical revelation of iron in nanoparticle-labelled 3 T6 fibroblast cultures: iron is associated with cells and the underlying glass substrate is mostly devoid of nanoparticle aggregates. On the higher magnification image seen in Fig. 8, Perls-stained clusters of nanoparticles can be noticed around the nucleus, probably corresponding to endocytic vesicles in the cytoplasm.

4. CONCLUSIONS

In this study we describe a simple method for the production of coated iron oxide nanoparticles at the gram scale with a stabilization shell based on carboxysilane. Surface modification is characterized by a shift to acidic pH of the isoelectrical point after coating. PCS and AFM measurements suggest that the stabilization shell is thin. Magnetometry indicates that the coating does not modify the magnetic properties of the iron oxide core. NPs derivatized by carboxysilane present interesting

stability properties. An aqueous solution of electrostatically stabilized NPs can be concentrated up to 70 wt% with many prospective applications in the field of true ferrofluids. In addition, NPs form large aggregates in DMEM, which favours their interaction with cultured adherent cells. These aggregates are redispersible in PBS, which confers to carboxysilane coated nanoparticles interesting properties for nonspecific cell labelling. For *in vivo* cell tracking applications, it is important to use magnetically tagged cells having no contrast agent stuck to their membrane. Our NPs have the advantage of offering stability and redispersibility in PBS. After eliminating the supernatant, a few millilitres of PBS can be added to dissolve the precipitate and form a clear solution. The hydrodynamic size of NPs in solution is <100 nm and is about 20–25 nm even in intensity representation mode after a few minutes in PBS. Thus, for cell labelling, aggregates of NPs can be removed during the PBS washing steps after the incubation period in order to obtain properly labelled cells.

ACKNOWLEDGEMENT

The authors thank Isabelle Mahieu, Corinne Pierart and Alain Roch for their help and discussions. This work is supported by the European Network for Cell Imaging and Tracking Expertise (ENCITE) and the Fonds de la Recherche Scientifique (FNRS). ENCITE is supported by the 7th Framework Program of the European Commission. P.L. is 'Chercheur Qualifié du Fonds National de la Recherche Scientifique (FRS-FNRS) – Belgium'. D. S. thanks the Walloon Region for the funding (First spin-off program). The authors thank the framework of COST D38 (Metal-Based Systems for Molecular Imaging Applications) and TD1004 (Theragnostics), the European Network of Excellence EMIL (European Molecular Imaging Laboratories) program LSCH-2004-503569, the Center for Microscopy and Molecular Imaging (supported by the European Regional Development Fund, the Walloon Region) and the Interuniversity Attraction Poles of the Belgian Federal Science Policy Office; contract/grant numbers P6/29 and P7/11, for their support.

REFERENCES

1. Bruchez M, Moronne M, Gin P, Weiss S, Alivisatos AP. Semiconductor nanocrystals as fluorescent biological labels. Science 1998; 281: 2013–2016.
2. Michalet X, Pinaud FF, Bentolila LA, Tsay JM, Doose S, Li JJ, Sundaresan G, Wu AM, Gambhir SS, Weiss S. Quantum dots for live cells, in vivo imaging, and diagnostics. Science 2005; 307: 538–544.
3. Couvreur P, Vauthier C. Nanotechnology: intelligent design to treat complex disease. Pharm Res 2006; 23: 1417–1450.
4. Kim J, Piao Y, Hyeon T. Multifunctional nanostructural materials for multimodal imaging, and simultaneous imaging and therapy. Chem Soc Rev 2009; 38: 372–390.
5. Gossuin Y, Gillis P, Hocq A, Vuong QL, Roch A. Magnetic resonance relaxation properties of superparamagnetic particles. WIREs: Nanomed Nanobiotechnol 2009; 1: 299–310.
6. Laurent S, Boutry S, Mahieu I, Vander Elst L, Muller RN. Iron oxide based MR contrast agents: from chemistry to cell labeling. Curr Med Chem 2009; 16: 4712–4727.
7. Hoehn M, Wiedermann D, Justicia C, Ramos-Cabrer P, Kruttwig K, Farr T, Himmelreich U. Cell tracking using magnetic resonance imaging. J Physiol 2007; 584: 25–30.
8. Kiessling F. Noninvasive cell tracking. Handb Exp Pharmacol 2008: 305–321.
9. Mailänder V, Landfester K. Interaction of nanoparticles with cells. Biomacromolecules 2009; 10: 2379–2400.
10. Petri-Fink A, Hofmann H. Superparamagnetic iron oxide nanoparticles (SPIONs): from synthesis to in vivo studies – a summary of the synthesis, characterization, in vitro, and in vivo investigations of SPIONs with particular focus on surface and colloidal properties. IEEE Trans Nanobiosci 2007; 6: 289–297.
11. Namkung S, Zech CJ, Helmberger T, Reiser MF, Schoenberg SO. Superparamagnetic iron oxide (SPIO)-enhanced liver MRI with ferucarbotran: efficacy for characterization of focal liver lesions. J Magn Reson Imag 2007; 25: 755–765.
12. Bulte JW. In vivo MRI cell tracking: clinical studies. Am J Roentgenol 2009; 193: 314–325.
13. Mailänder V, Lorenz MR, Holzapfel V, Musyanovych A, Fuchs K, Wiesneth M, Walther P, Landfester K, Schrezenmeier H. Carboxylated superparamagnetic iron oxide particles label cells intracellularly without transfection agents. Mol Imag Biol 2008; 10: 138–146.
14. Boutry S, Brunin S, Mahieu I, Laurent S, Vander Elst L, Muller RN. Magnetic labeling of non-phagocytic adherent cells with iron oxide nanoparticles: a comprehensive study. Contrast Media Mol Imag 2008; 3: 223–232.
15. van Buul GM, Farrell E, Kops N, van Tiel ST, Bos PK, Weinans H, Krestin GP, van Osch GJVM, Bernsen MR. Ferumoxides-protamine sulfate is more effective than ferucarbotran for cell labeling: implications for clinically applicable cell tracking using MRI. Contrast Media Mol Imag 2009; 4: 230–236.
16. Monet-Abou K, Montet X, Weissleder R, Josephson L. Transfection agent induced nanoparticle cell loading. J Mol Imag 2005; 4: 165–171.
17. Limbach LK, Li Y, Grass RN, Brunner TJ, Hintermann MA, Muller M, Gunther D, Stark W. Oxide nanoparticle uptake in human lung fibroblasts: effects of particle size, agglomeration, and diffusion at low concentrations. J Environ Sci Technol 2005; 39: 9370–9376.
18. Wilhelm C, Billotey C, Roger J, Pons JN, Bacri JC, Gazeau F. Intracellular uptake of anionic superparamagnetic nanoparticles as a function of their surface coating. Biomaterials 2003; 24: 1001–1011.
19. Forge D, Roch A, Laurent S, Tellez H, Gossuin Y, Renaux F, Vander Elst L, Muller RN. Optimization of the synthesis of superparamagnetic contrast agents by the design of experiments method. J Phys Chem C 2008; 112: 19178–19185.
20. Thorek DLJ, Chen AK, Czupryna J, Tsourkas A. Superparamagnetic iron oxide nanoparticle probes for molecular imaging. Ann Biomed Eng 2006; 34: 23–38.
21. Gupta AK, Gupta M. Cytotoxicity suppression and cellular uptake enhancement of surface modified magnetic nanoparticles. Biomaterials 2005; 26: 1565–1573.
22. Laurent S, Bridot J-L, Vander Elst L, Muller RN. Magnetic iron oxide nanoparticles for biomedical applications. Fut Med Chem 2010; 2: 427–449.
23. Laurent S, Forge D, Port M, Roch A, Robic C, Vander Elst L, Muller RN. Magnetic iron oxide nanoparticles: synthesis, stabilization, vectorization, physico-chemical characterizations and biological applications. Chem Rev 2008; 108(6): 2064–2110.
24. Nobbmann U, Morfesis A. Light scattering and nanoparticles. Mater Today 2009; 12(5): 52–54.
25. Roch A, Gossuin Y, Muller RN, Gillis P. Superparamagnetic colloid suspensions: water magnetic relaxation and clustering. J Magn Magn Mater 2005; 293: 532–539.
26. Daou TJ, Grene`che JM, Pourroy G, Buathong S, Derory A, Ulhaq-Bouillet C, Donnio B, Guillon D, Begin-Colin S. Coupling agent effect on magnetic properties of functionalized magnetite-based nanoparticles. Chem Mater 2008; 20: 5869–5875.
27. Lee N, Choi Y, Lee Y, Park M, Moon WK, Choi SH, Hyeon T. Water-dispersible ferrimagnetic iron oxide nanocubes with extremely high r_2 relaxivity for highly sensitive in vivo MRI of tumors. Nano Lett 2012; 12: 3127–3131.
28. Pöselt E, Kloust H, Tromsdorf U, Janschel M, Hahn C, Maßlo C, Weller H. Relaxivity optimization of a PEGylated iron-oxide-based negative magnetic resonance contrast agent for T_2-weighted spin-echo imaging. ACS Nano 2012; 6: 1619–1624.

29. Tong S, Hou S, Zheng Z, Zhou J, Bao G. Coating optimization of superparamagnetic iron oxide nanoparticles for high T_2 relaxivity. Nano Lett 2010; 10: 4607–4613.
30. Jung CW, Jacobs P. Physical and chemical properties of superparamagnetic iron oxide MR contrast agents: ferumoxides, ferumoxtran, ferumoxsil. Magn Reson Imag 1995; 13: 661–674.
31. Lee H, Lee E, Kim DK, Jang NK, Jeong YY, Jon S. Antibiofouling polymer-coated superparamagnetic iron oxide nanoparticles as potential magnetic resonance contrast agents for in vivo cancer imaging. J Am Chem Soc 2006; 128: 7383–7389.
32. Jain N, Wang Y, Jones SK, Hawkett BS, Warr GG. Optimized steric stabilization of aqueous ferrofluids and magnetic nanoparticles. Langmuir 2010; 26: 4465–4472.
33. Harris LA, Goff JD, Carmichael AY, Riffle JS, Harburn JJ, St. Pierre TG, Saunders M. Magnetite nanoparticle dispersions stabilized with triblock copolymers. Chem Mater 2003; 15(6): 1367–1377.
34. Goodwin J. Colloid and Interfaces with Surfactant and Polymers, an Introduction. Wiley: New York, 2004.
35. Janic B, Rad AM, Jordan EK, Iskander ASM, Ali Md M, Varma NRS, Frank JA, Arbab AS. Optimization and validation of FePro cell labeling method. PLoS One 2009; 4(6): e5873.

SUPPORTING INFORMATION

Supporting information can be found in the online version of this article.